Analysis Method for the Low-Order Resistive Interchange Instability in LHD with Stochastic Magnetic Field Line Structure[*]

Ryosuke UEDA, Masahiko SATO[1], Kiyomasa WATANABE[1], Yutaka MATSUMOTO,
Yasuhiro SUZUKI[1], Masafumi ITAGAKI, Shun-ichi OIKAWA and Yasushi TODO[1]

Graduate School of Engineering Hokkaido University, Sapporo 060-8628, Japan
[1]*National Institute for Fusion Science, 322-6 Oroshi-cho, Toki 509-5292, Japan*

In Large Helical Device experiments, independent low-order magnetic fluctuations due to the resistive interchange mode are commonly observed; investigating the characteristics of this instability is our ultimate goal. Two new methods for analyzing the single low-order instability in the stochastic region are developed. One method investigates it by constructing the initial single-mode perturbation. The other method investigates it by constructing a reference surface outside the last closed flux surface. The reference surface is necessary for constructing the coordinates that are used to extract the Fourier mode in the stochastic field line structure.

1. Introduction

In high-β Large Helical Device (LHD) experiments, independent low-order magnetic fluctuations that resonate with the rational surface are commonly observed [1]. The dependence on the β value and magnetic Reynolds number suggests that such magnetic fluctuations are due to the resistive interchange mode. This mode is unstable in the magnetic hill region. The entire LHD plasma region typically has a magnetic hill configuration with low β. As the β value increases, a magnetic well is formed in the core region, whereas the magnetic hill remains in the peripheral region. Thus, the suppression of the resistive interchange mode in the peripheral region is thought to be important in high-β operations. On the other hand, theoretical studies predict that the structure of the magnetic surfaces is destroyed with increasing β, and turns into the stochastic state. Therefore, to study the properties of magnetohydrodynamics (MHD) stability in prospective LHD-type fusion reactors, it is important to investigate the characteristics of the resistive interchange mode in the stochastic magnetic field line structure.

The interchange mode in helical-type plasma similar to that in the LHD has been studied theoretically. Many of these studies used numerical analysis codes, e.g., TERPSICHORE [2], CAS3D [3], and NORM [4], based on the magnetic coordinates. However, to investigate the properties of the resistive interchange mode in the stochastic region, we should use real coordinates in the MHD

stability analysis code that handles the equilibrium with the stochastic magnetic field line structure. Recently, the MHD Infrastructure for Plasma Simulation (MIPS) code [5, 6] was developed, and an early study of the nonlinear MHD saturation process in high-β LHD plasma was presented [6]. The study predicts that the ballooning modes with a medium mode number are the most unstable and saturated, maintaining the pressure gradient when the plasma has a high magnetic Reynolds number. Because low-order magnetic fluctuations that resonate with the rational surface are observed in LHD experiments, we focus on the characteristics of the resistive interchange instability with the low-order mode, which is the same as that observed in the experiments.

To analyze the independent low-order unstable mode in the stochastic magnetic field line structure, two issues must be resolved. One is the development of a method for investigating the specified single-mode instability. Although the original MIPS procedure employs random perturbation of the initial conditions, this perturbation has multiple modes, including both stable and unstable ones. Because stable modes exist, considerable computational time is required until the growth of unstable modes appear clearly. The existence of multiple unstable modes poses a problem in that we cannot investigate the specified single unstable mode. In section 2, these problems are resolved by describing a single-mode perturbation in Boozer coordinates [7]. The other issue to be resolved is to define "quasi-magnetic" coordinates based on reference surfaces to describe a single-mode perturbation outside the Last Closed Flux Surface (LCFS). The use of the

VMEC code [8] is one way to construct Boozer coordinates. The fixed-boundary VMEC code requires the shape of the LCFS as input. However, in the stochastic magnetic field line structure outside the LCFS, the magnetic surfaces cannot be obtained by magnetic field line tracing. Without the coordinates, we cannot describe the single-mode perturbation in the stochastic field line structure. In section 3, reference closed surfaces outside the LCFS obtained by using the Radial Basis Function (RBF) expansion method [10] are defined. Although these reference surfaces outside LCFS are not physical, we use the surfaces as the fixed-boundary in the VMEC code to obtain Boozer-like coordinates. Using these Boozer-like coordinates, we describe a single-mode perturbation outside the LCFS.

2. Development of the Initial Mode Perturbation Method

As mentioned in the previous section, issues with the original procedure in the MIPS code need to be resolved, because this procedure cannot analyze a specified single-mode instability. To resolve these issues, an initial single-mode perturbation method was developed. In this method, the perturbation having a specified single unstable mode is described in Boozer coordinates. Without any other unstable mode, the only constructed single unstable mode is expected to grow. In addition, without the stable mode, the linear growth of the constructed single-mode instability can be seen shortly after the beginning of the calculation, which reduces the computational time.

2.1 Method of constructing mode perturbation

The described mode structure in Boozer coordinates is based on our knowledge of the linear analysis of the resistive interchange mode. The typical resistive interchange mode structure of heliotron plasma is obtained by solving the eigenvalue equations based on the reduced MHD equations in the straight heliotron geometry. Figure 1 shows the resistive interchange mode structure of the pressure. The poloidal mode number $m = 2$ and toroidal mode number $n = 1$ are used. The rational surface is located around $\rho = 0.4$. The mode structure has a peak value around the rational surface. From this result, we model the structure of the mode perturbation in Boozer coordinates as a Gaussian profile:

$$\tilde{P}(\psi) = A_{\mathrm{amp}} \exp\left[-\left(\frac{\rho - \rho_{\mathrm{s}}}{\sigma}\right)^2\right]. \qquad (1)$$

Here A_{amp} is the amplitude of the perturbation, and ρ_{s} denotes the location of the rational surface. The width of the mode structure is conditioned by the σ value. In this study, $A_{\mathrm{amp}} = 10^{-7}$ and $\sigma = 0.05$ are used. ρ_{s} depends on the rotational transform profile obtained at equilibrium. The equilibrium profile is constructed by the HINT code [9]. Figure 2 shows the modeled mode structure. Because the MIPS code takes the initial conditions in real coordinates,
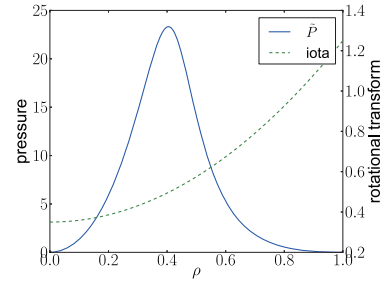

Fig. 1 Resistive interchange mode structure of the pressure obtained by eigenmode analysis in straight heliotron plasma.
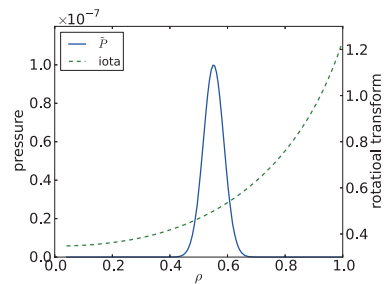

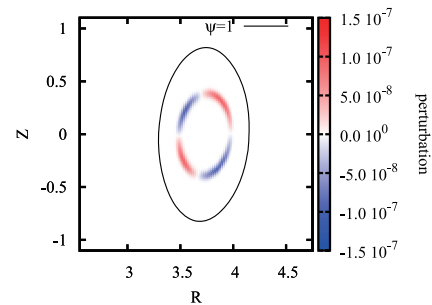Fig. 2 Mode structure model of pressure for the initial mode perturbation.

Fig. 3 Mode perturbation of pressure in real coordinates in a vertically elongated cross section. Closed solid line denotes $\psi = 1$ ($\rho = 1$).

the mode perturbation built in Boozer coordinates is converted to that in real coordinates. Figure 3 shows the perturbation on the vertically elongated cross section.

2.2 Growth of mode perturbation

The governing MHD equations in MIPS are as follows:

$$\frac{\partial p}{\partial t} = -\nabla \cdot (\rho \boldsymbol{v}) - (\gamma - 1)p\nabla \cdot \boldsymbol{v}$$
$$+ (\gamma - 1)\left[\nu \rho w^2 + \frac{4}{3}\nu\rho(\nabla \cdot \boldsymbol{v})^2 + \eta \boldsymbol{j} \cdot (\boldsymbol{j} - \boldsymbol{j}_{\mathrm{eq}})\right], \qquad (2)$$

$$\rho \frac{\partial}{\partial t}\boldsymbol{v} = -\rho \boldsymbol{w} \times \boldsymbol{v} - \rho\nabla\left(\frac{v^2}{2}\right) - \nabla p$$
$$+ \boldsymbol{j} \times \boldsymbol{B} + \frac{4}{3}\nabla[\nu\rho(\nabla \cdot \boldsymbol{v})] - \nabla \times [\nu\rho \boldsymbol{w}], \qquad (3)$$
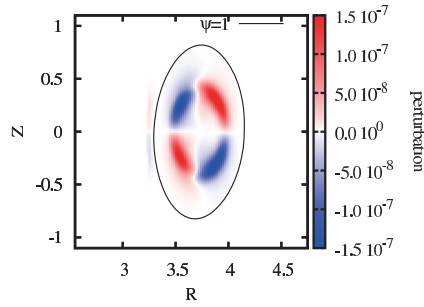
Fig. 4　Pressure perturbation at 30,000 time steps. Magnetic Reynolds number is $S = 10^6$.
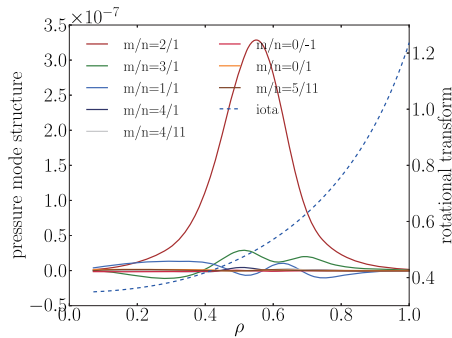

Fig. 5　Mode structures of the perturbation at 30,000 time steps. Magnetic Reynolds number is $S = 10^6$.

$$\frac{\partial \rho}{\partial t} = -\nabla \cdot (\rho \boldsymbol{v}), \tag{4}$$

$$\boldsymbol{w} = \nabla \times \boldsymbol{v}, \tag{5}$$

$$\boldsymbol{j} = \frac{1}{\mu_0} \nabla \times \boldsymbol{B}, \tag{6}$$

$$\frac{\partial \boldsymbol{B}}{\partial t} = -\nabla \times \boldsymbol{E}, \tag{7}$$

$$\boldsymbol{E} = -\boldsymbol{v} \times \boldsymbol{B} + \eta(\boldsymbol{j} - \boldsymbol{j}_{\text{eq}}). \tag{8}$$

The meanings of variables are the same as in Ref. [5]. The time evolution of mode perturbation was computed. The resolutions are 128×128 on the poloidal section and 256 along the toroidal direction. In the poloidal section, the computational area is set to $2.55 \leq R \leq 4.75$ and $-1.1 \leq Z \leq 1.1$. The magnetic Reynolds number and β value are $S = 10^6$ and $\langle \beta \rangle = 2\%$, respectively. The initial perturbation has the single $(m, n) = (2, 1)$ mode shown in Fig. 3. Figure 4 shows the pressure perturbation at 30,000 time steps (133 Alfvén times) on the vertical cross section. It can be seen that the initial mode perturbation grows. A mode analysis of the perturbation was performed, and the perturbation profile in real coordinates was mapped to Boozer coordinates. The eight largest structures of the analyzed mode are shown in Fig. 5. Among them, the $(m, n) = (2, 1)$ mode structure clearly has the largest amplitude. Figure 6 shows the time evolution of kinetic energy as a function of the time step. Under random perturbation
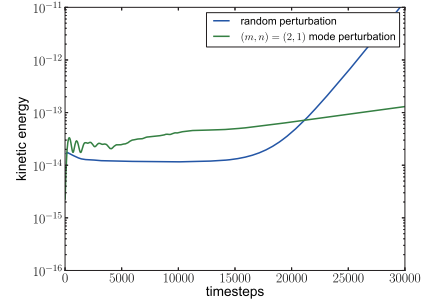

Fig. 6　Time evolution of kinetic energy. Green and blue lines denote the $(2, 1)$ mode perturbation and random perturbation, respectively.

(blue), the time evolution of the kinetic energy decreases until around 15,000 time steps, and then the linear growth phase appears. In contrast, under the $(2, 1)$ mode perturbation (green), the linear growth phase appears after around 5000 time steps. The mode perturbation is found to make the linear phase appear in fewer time steps. The rate of change of the kinetic energy depends on the growth rate. The linear growth rate under random perturbation is larger than under the $(2, 1)$ mode perturbation. Thus, random perturbation includes various unstable modes. These include unstable modes whose growth rate is greater than that of the $(2, 1)$ mode.

3. Construction of the Reference Surfaces in the Stochastic Magnetic Field Line Structure

Once the MHD equilibrium is calculated by the VMEC code, Boozer coordinates are easily constructed by using a transformation between the magnetic coordinates (VMEC coordinates and Boozer ones) [7, 8]. Normally, Boozer coordinates are defined when magnetic surfaces exist. However, we assume that quasi-magnetic surfaces exist in the stochastic region, which means that the MHD equilibrium force balance is almost satisfied there. Quasi-MHD equilibrium configurations are obtained by the VMEC code, and Boozer-like coordinates can be defined in the stochastic region. To calculate the quasi-MHD equilibrium configurations by the VMEC code, the shape of the boundary is required as input data. In the conventional use of VMEC, the LCFS is adopted as the boundary. In contrast, this study uses the quasi-magnetic surface [10] and constructs Boozer-like coordinates in the stochastic region. The shape of the largest boundary should be extracted from the quasi-magnetic surfaces for the VMEC input. However, the boundary has to be a common surface in every poloidal section. In addition, when carrying out the VMEC code, the input data are given in VMEC coordinates. Therefore, this section descrived a method for extracting the boundary shape in the stochastic region and transforming the boundary shape in real coordinates to that in VMEC coordinates.

(a) RBF cxpansion   (b) Comparison between LCFS
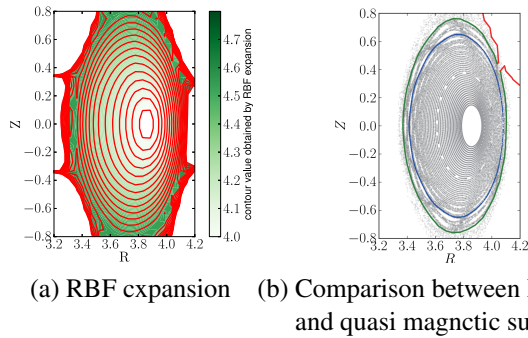   and quasi magnctic surface

Fig. 7   (a) Contour map (green) and lines (red) constructed by
the RBF expansion method. (b) Comparison of LCFS
(blue) and quasi-magnetic surface (green, red). One con-
tour line is almost closed line (green). However, part of
the line is open (red).

Fig. 8   Boundary geometry on poloidal sections at toroidal an-
gles of 0, 5.4°, 10.8°, and 18°, constructed by the RBF
expansion method (circles) or Fourier components in
VMEC coordinates (red lines).

3.1   RBF expansion method for constructing quasi-magnetic surfaces

Using the RBF expansion method [10], we fit the
group of discrete points by tracing a magnetic field line on
a poloidal cross section to a continuous curve. The curve is
recognized as a quasi-magnetic surface. Within the LCFS,
the curves almost coincide wth the magnetic surfaces ob-
tained by magnetic line tracing. In this study, the start
points of the magnetic field line tracing for the RBF ex-
pansion method are

$$(R_{start}, Z_{start}) = (4.0 + 0.01k, 0), \quad k = 0, 1, \ldots, 70,$$
(9)

in the horizontally elongated poloidal cross section. The
magnetic field configuration at finite beta is calculated by
the HINT code [9]. The centers of the RBFs are distributed
on grids in the $(2.2 < R < 5.2, -1.5 < Z < 1.5)$ region with
a grid spacing of $\Delta = 0.3$. We adopt the Gaussian function
as the RBF, as in Itagaki's study. The scaling factor of the
RBF function is $\sigma = 1.0$. Figure 7 (a) shows the contour
map (green) and contour lines (red) obtained by the RBF
expansion method.

3.2   Extracting the quasi-magnetic surfaces for boundary geometry

Figure 7 (b) shows the larger and almost closed line
(green, red) that is extracted from the contour line in
Fig. 7 (a). The red line is the open part of the contour
line, which is removed and interpolated so that the con-
tour line becomes closed. Further, the Poincaré plot is also
drawn. In particular, the blue line shows the LCFS, which
is the magnetic field line trace originating at the start point
$R = 4.39$. Similarly, we obtain the quasi-magnetic surfaces
in the stochastic region on 11 poloidal sections at toroidal
angles of $0° - 18°$. However, every reference surface has
to constitute the same quasi-magnetic surface. Figure 7 (b)
shows that the reference surface (green line) obtained by
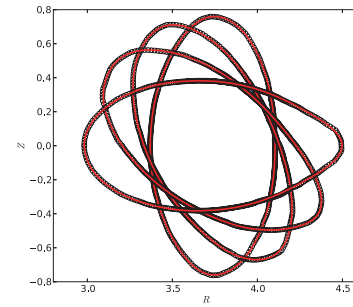the RBF expansion method has a larger geometry than the

LCFS (blue line) and includes the region with the stochas-
tic magnetic field line structure.

3.3   Representation of the quasi magnetic surface in VMEC coordinates

To deal with the quasi magnetic-surface as VMEC in-
put, we have to represent the constructed boundary geom-
etry in VMEC coordinates. The real coordinates are trans-
formed to VMEC coordinates using the KFIT code, which
is an improved version of DESCUR [11]. Using this code,
we can obtain the Fourier representation for boundary ge-
ometry. Figure 8 shows the boundary geometries obtained
by the Fourier representations in VMEC coordinates (red)
and those obtained by the RBF expansion method (circles)
at toroidal angles of 0, 5.4°, 10.8° and 18°. It can be seen
that the two geometries are almost the same. The VMEC
coordinates are accurately constructed outside the LCFS.
Using the routine that transforms VMEC coordinates to
Boozer coordinates, we can obtain Boozer-like coordinates
including the stochastic region.

4. Summary

Two techniques developed for the analyses of the
independent low-order magnetic fluctuation observed in
LHD experiments are described. One is a method of linear
analysis of a single low-order mode instability. This tech-
nique enables us to analyze a specified single low-order
mode and reduces the computational time. The other is a
method for constructing reference surfaces in the stochas-
tic magnetic field line structure using the RBF expansion
method. This enables us to obtain the reference surface
outside the LCFS, which can be reconstructed in VMEC
coordinates using the KFIT code. Using these techniques,
we will construct the initial single-mode perturbation in a
larger region than the LCFS. The qualitative characteristics
of the low-order magnetic fluctuations will be investigated.
Further, this achievement will contribute to the clarifica-
tion of the mechanism that causes the low-order magnetic
fluctuation.

[1] K.Y. Watanabe *et al.*, Phys. Plasmas **18**, 056119 (2011).
[2] W.A. Copper, Plasma Phys. Control. Fusion **34**, 1011 (1992).
[3] C. Nührenberg, Phys. Plasmas **6**, 137 (1999).
[4] K. Ichiguchi, N. Nakajima, M. Wakatani *et al.*, Nucl. Fusion **43**, 1011 (2003).
[5] Y. Todo, N. Nakajima, M. Sato and H. Miura, Plasma Fusion Res. **5**, S2062 (2010).
[6] M. Sato, N. Nakajima, K.Y. Watanabe *et al.*, 24th IAEA FEC 2012, TH/P3-25 (2012).
[7] A.H. Boozer, Phys. Fluids **24**, 1999 (1981).
[8] S.P. Hirshman, W.I. van Rij and P. Merkel, Comput. Phys. Commun. **43**, 143 (1986).
[9] K. Harafujim T. Hayashi and T. Sato, J. Comput. Phys. **81**, 169 (1989).
[10] M. Itagaki, G. Okubo, M. Akazawa *et al.*, Plasma Phys. Control. Fusion **54**, 125003 (2012).
[11] S.P. Hirshman *et al.*, Phys. Fluids **28**, 1387 (1985).